ELSEVIER

Fusion Engineering and Design 37 (1997) 455–463

Fusion Engineering and Design

Sputtering erosion of beryllium coated plasma facing components—general considerations and analysis for ITER detached plasma regime[1]

Jeffrey N. Brooks [a,*], David N. Ruzic [b], Douglas B. Hayden [b]

[a] *Argonne National Laboratory, 9700 S. Cass Ave., Argonne, IL 60439, USA*
[b] *University of Illinois, 103 S. Goodwin Ave., Urbana, IL 61801, USA*

Abstract

Sputtering erosion is a key performance issue for beryllium coatings in future fusion reactors. Past analysis of this subject for various edge plasma regimes—as briefly reviewed here—shows acceptable erosion only for low duty factor devices. Erosion analysis is now focusing on a very low boundary temperature (≤ 2 eV) 'detached plasma' regime for the International Thermonuclear Experimental Reactor (ITER) Vertical Director design. Erosion and tritium codeposition calculations are made for this regime using a coupled WBC/REDEP/DEGAS$^+$ code analysis. The analysis includes calculations of low energy, oblique incidence, sputtering yields using the VFTRIM-3D code calibrated to fit recent data on D–Be sputtering. We find that beryllium performs better than carbon for detached conditions due to the absence of chemical sputtering. Beryllium performs worse than vanadium or tungsten. Net erosion rates of beryllium coated first wall components, due mainly to physical sputtering by charge exchange D–T neutrals, vary from ~ 0 to 2 cm per burn-year along the wall. Tritium co-deposition in redeposited beryllium surface layers may be high. © 1997 Elsevier Science S.A.

Keywords: Sputtering; Erosion; Beryllium; Detached plasma

1. Introduction

As discussed throughout this special issue, beryllium offers several advantages as a plasma facing material, including low core plasma radiation, probable absence of runaway self-sputtering, oxygen gettering ability, and in-situ recoating capability. A key disadvantage of beryllium, however, is potentially high sputtering erosion. Another concern is tritium codeposition in growing redeposited beryllium surface layers. A simple observation about beryllium erosion is that hydrogen isotope and helium sputtering coefficients are high, over a broad energy range, relative to other materials. This follows from beryllium's low surface binding energy and low atomic mass. Also, redeposition fractions for sputtered Be atoms are relatively low due to higher surface emission velocities (scaling with atomic mass as $\sim m^{-0.5}$) and a lower ionization rate coefficient.

* Corresponding author.

[1] Work supported by the Office of Fusion Energy, U.S. Department of Energy.

PII S0920-3796(97)00090-2

Therefore, Be faces a challenge to be competitive, from an erosion standpoint, with most other materials.

In spite of high erosion rates, beryllium, as well as carbon, has been considered for next-generation, low duty factor devices such as ITER. As with present tokamaks, both materials may serve acceptably in this role. High-Z materials, or liquid metals, however, may be the only feasible plasma facing materials for demonstration and commercial fusion reactors. These are not without problems of their own. The key challenge to using beryllium for high duty-factor devices is to identify plasma edge regimes that result in acceptable erosion performance. As part of this effort we examine erosion performance for a detached plasma regime. As a follow-up to Ref. [1] which initiated analysis of the divertor target erosion for this regime, we concentrate here on first wall erosion. Due to numerous plasma-model uncertainties for this regime our intent is to provide a scoping analysis—that is to define trends and suggest future research needs. More analysis and data will be needed to develop detailed design information for fusion reactors.

2. Review of beryllium erosion analysis

2.1. Computational methods

Sputtering erosion in magnetic fusion devices is governed by the erosion/redeposition process in which the net erosion rate is determined by the wide-area convolution of D, T, and He sputtering, self-sputtering, and impurity transport in the sheath, near-surface region, scrape-off layer, and core plasma [2]. Models and computational methods for analysis of erosion/redeposition are summarized in Ref. [3]. Codes in use include the REDEP [2,4] large-area erosion/redeposition code, the WBC [5] sub-gyro orbit resolution impurity transport code, the B-PHI [6] sheath code, and the VFTRIM-3D [7,8] rough-surface sputtering code. The erosion codes are used with input of two-dimensional profiles of plasma parameters, magnetic field, surface geometry, and boundary conditions. In addition to erosion rates, a code such as REDEP computes the amount of tritium codeposited on the boundary surfaces, using models for surface-temperature-dependent hydrogen retention rates. The current of sputtered material entering the core plasma—a measure of core plasma contamination potential—is also computed.

Erosion code validation efforts have been performed in various devices including TFTR [9], DIII-D [10,11], PISCES [12], and ASDEX Upgrade [13]. These studies have shown generally good agreement between predicted and measured absolute erosion rates and/or redeposition profiles, thereby providing reasonable confidence in the predictive value of the codes—providing, of course, that the input plasma solution is valid. Major uncertainties for future devices include the properties (sputtering, adhesion, etc.) of thick redeposited films, and the effects of multi-material (C, Be, W, O, etc.) mixing on sputtering and tritium codeposition properties.

2.2. Fusion reactor erosion studies

In this section we summarize the erosion analysis of several tokamak reactor designs in which beryllium was considered as a plasma facing material. Table 1 shows selected results from these studies [2,4,14,15] in terms of peak net erosion rate for the component in question, and the sputtering erosion lifetime of a 5 mm thickness of Be coating. (An additional thickness will also be needed to account for disruption erosion.) These studies span a range of plasma facing component types and plasma edge regimes. The plasma regimes are roughly characterized by the peak plasma electron temperature at the boundary. The credibility of the plasma models in these studies vary—some are the results of detailed 2-D plasma transport calculations and others are based on simple parametric models. Although all of the devices listed are experimental devices, we show erosion lifetime on the basis of an extrapolated high duty factor, as would apply to a commercial fusion reactor.

These results show possibly acceptable beryllium lifetimes for low duty-factor (several percent) experimental devices—with the proper choice of

Table 1
Erosion analysis summary of several fusion reactor design studies for beryllium coated plasma facing components

Design study	Plasma facing component	Plasma edge regime	Peak electron temperature at boundary, eV	Peak net erosion rate (cm/burn year)	Erosion lifetime of 5 mm Be coating @100% duty factor	Comments
FED/INTOR [2]	Pumped limiter	High recycle	20	7	~1 month	
		Very high temperature	700	5	~1 month	Highly speculative regime
TPX [14]	Divertor	High temperature	120	221	≡1 day	Steady-state compatible regime
ITER [4]	Divertor	High recycle	30	49	~4 days	
ITER [15]	'Gas bag' type divertor	Dissipative-gas target	70	689	~6 h	Low redeposition configuration

plasma regime—but not for commercial reactor operation. The lifetime results for carbon (not shown) are generally somewhat better (factor of ~ 2) but qualitatively similar. The results for high-Z materials depend on the regime. For boundary plasma temperatures below about 50 eV tungsten erosion is much lower (orders-of-magnitude) than the low-Z materials. At high temperatures, for example the TPX case, runaway self-sputtering occurs for tungsten and vanadium. (Thus, there is no high-lifetime material identified for a TPX type, non-inductive current drive compatible edge regime—except possibly for a liquid metal system).

Another issue is core plasma contamination from sputtering. For a tungsten coated divertor, for non-runaway regimes, the predicted contamination is essentially zero. This is due to the complete ionization of sputtered tungsten in the near-surface (0–3 cm) region of the divertor plate, and subsequent redeposition to the surface. In contrast for beryllium (and carbon), several percent of the sputtered material typically enters the core plasma—this is a tolerable amount.

These studies focused on the critical issue of burn-phase erosion of the main particle/heat handling surface, i.e. the divertor or pumped limiter. Other, generally less analyzed issues, are first wall erosion, startup period erosion, and erosion of disruption transported material.

3. ITER detached plasma erosion analysis

3.1. Model

We are examining erosion of the divertor and first wall of the ITER Vertical Divertor design [16]. This work extends the initial analysis [1] to the first wall. The boundary model for the calculations is shown in Fig. 1. The first wall region examined extends from the top of the outer divertor to about the outer midplane and includes the startup limiter and baffle components. For the tritium codeposition calculation we scale erosion results to include both inner and outer lower-half wall regions. Erosion analysis of the upper-half wall is planned for the future.

The detached plasma solution used here is given by the B2/EIRENRE code analysis of Kukushkin et al. [17]. This solution is characterized by ion and electron temperatures of 1–2 eV and electron densities of $\sim 10^{19}$–10^{21} m^{-3} at and along the $\sim$1-m divertor plate. The boundary plasma temperatures increase gradually to ~ 10 eV at the wall near the midplane, but with much lower ($\sim 10^{18}$–10^{19} m^{-3}) plasma densities. The plasma solution [17] contains the 2-dimensional profiles of plasma ion and electron densities and temperature for the ITER scrapeoff layer. The profiles are used as input to the DEGAS^{+} Monte-Carlo neutrals code and to the WBC and REDEP impurity transport codes. The WBC code is used here for very detailed calculations, including in particular the sub-gyro orbit motion of sputtered particles, at selected points along the wall. The detailed WBC results, for instance on the redeposited charge state and angular distributions, are incorporated into REDEP which is then used for erosion analysis of the entire surface.

For carbon chemical sputtering calculations thermal methane is launched, and carbon/hydrocarbon particles collide with the plasma through elastic and inelastic collisions, and undergo Lorentz force motion. Ref. [18] gives details of hydrocarbon transport models used in the WBC code. An update is the inclusion of elastic colli-

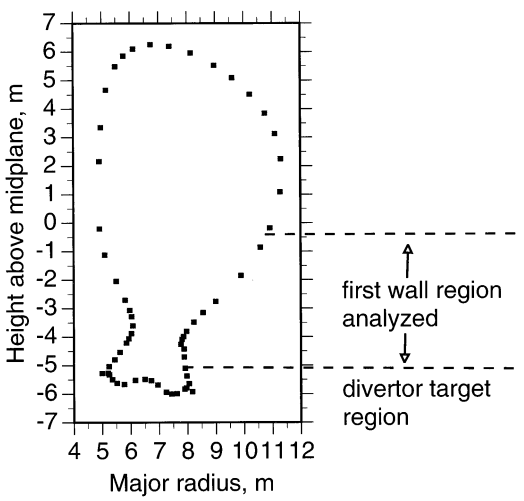

Fig. 1. Computational grid for boundary erosion calculations.

sions between hydrocarbons and D–T ions and neutrals. The 34 atomic and molecular reactions of Ref. [19] are followed. Redeposited particles stick or are reemitted according to the species-dependent model of Ref. [18], such model tending to be confirmed by recent data [20].

The plasma analysis for this regime, by this [17] and other research groups, is still evolving and is speculative to various degrees. For purposes of examining erosion, however, the present solution should be reasonably typical. Also, in general, the plasma model for wall erosion calculations is more uncertain than for the divertor. In particular, the ion fluxes to the wall are not as well specified, depending on very shallow angle geometry effects. The sheath potential at the wall is also uncertain. For the present purposes we assume toroidal symmetry, a fixed near-tangential incident field angle, and a poloidally-varying sheath potential of 3 kT_e. Our erosion results are thus a toroidal average. The assumption of toroidal symmetry is most appropriate to the burn period case analyzed here. For the startup period involving high ion flux to the limiter, toroidal asymmetries are likely to produce significant deviations from the average behavior.

The DEGAS$^+$ code [21] is a Monte-Carlo neutral code which tracks neutral atoms and molecules from their source until they are ionized by the background plasma. All ionization, scattering and charge-exchange reactions between ions and neutrals are included. Special attention is paid to the interactions with the wall and elastic scattering of neutral atoms off the background neutral molecules. The code allows for detailed geometry and calculates local as well as global recycling of neutrals. The energy and angular spectra of all the neutral particles contacting the walls and other surfaces in the geometry are recorded. These are used as input to the REDEP and WBC codes. For this work the ITER geometry of the outer divertor from the midplane all the way into the pump duct was simulated. The DEGAS$^+$ code was applied to the plasma solution to compute, in detail, neutral hydrogen transport to the boundaries. For purposes of calculating particle reflection, the walls were taken to be beryllium. This introduced some error in the carbon and tungsten solutions but not in their gross behavior. Also, for this study the walls were modeled at the code-default value of 500°C, which is hotter than the actual temperature. Two other runs were made with lower wall temperatures to check the molecular flux. The high molecular flux value obtained was not due to the wall temperature, but rather the high ion flow velocity in the plasma background. The neutral source was recycling of the ion flux from the walls. Neutral exits were the main plasma and a small equivalent opening which represents the net pumping exhaust in the middle of the louvered wall.

With inputs of plasma parameters and neutral fluxes, the wall erosion was then computed by a combined WBC/REDEP analysis. For simplicity in making comparisons, a single coating material per analysis was used. In practice, several materials may be employed—in particular tungsten for the baffle region, carbon for the divertor target, and beryllium for the limiter and remaining wall have been proposed for ITER. For this study the near-surface transport ($\sim$0–3 cm) of sputtered material was followed in detail, however, atoms ionized past the near-surface region were only followed in an approximate manner. The related methodology used to compute the codeposited tritium due to wall sputtering will be described.

3.2. Oblique incidence beryllium sputtering yields

The REDEP code computes sputtering based on a convolution of incident particle energy (for ions, typically Maxwellian plus sheath-added energy) and angle of incidence. Sheath studies [6,22] have shown an average elevation incidence angle for tokamak divertor geometries of $\sim 60°$ from the normal (with standard deviation of $\sim 10°$), for impinging D^+, T^+, and He^+ ions. Atoms from charge exchange generally impact at an average of $\sim 45°$. There is thus a general need for sputtering coefficient data at oblique incidence, which is typically lacking, particularly at low energies. Code calculations are therefore needed to supplement of extend existing data.

In particular for this and other studies, VFTRIM-3D [7,8] is used to predict sputtering yields. The code is a variation of TRIM [23].

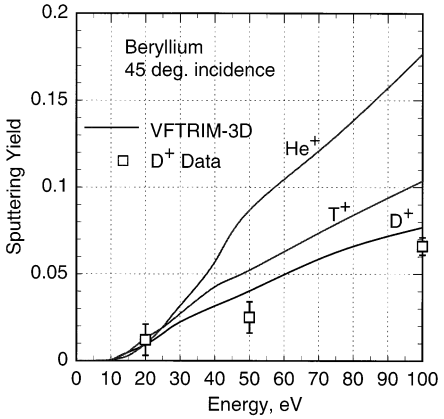

Fig. 2. VFTRIM-3D code calculated sputtering yields for beryllium. Surface binding energy adjusted to more accurately match experimental data [24,25].

VFTRIM-3D incorporates a fractal surface roughness model and has proven more accurate at low energies and non-normal incident angles [7]. New experimental data is also now available at 20 and 50 eV for D^+ on Be at 45° incidence [24] supplementing data for D^+ on Be at higher energies [25]. The simulation used here has the surface binding energy adjusted downward from 3.36 to 2.26 eV at energies below 100 eV to more accurately fit the experimental data. This is justified in part by molecular dynamic simulations [26] which show that the binding energy of atoms in protruding surface features is lowered on the order of 1 eV from the binding energy values of atoms on a flat surface, and that at lower energies the incident particles primarily interact only with the topmost layer.

The VFTRIM-3D results are shown in Fig. 2 for 45° incidence. The code results are a reasonably good match to the D on Be data at the energies indicated above. Calculations with other incident angles are planned. We have used these calculations in the present erosion estimates.

3.3. Neutral fluxes

DEGAS$^+$ results for the wall are shown in Fig. 3. The DEGAS$^+$ solution shows a total neutral atom current to the wall equal to about half of that on the divertor. Average neutral energies range from several eV at the divertor end to about 200 eV near the midplane. The latter energy is due to the fact that the charge exchange current, away from the divertor, arises from relatively hot regions of the plasma, the near-wall low-density plasma being fairly transparent to D–T neutrals.

A striking result of the DEGAS$^+$ solution is a high non-thermal D–T molecular current to the wall, of order $4\times$ the atomic current, and with energies in the 3–5 eV range. These are due to surface emitted thermal molecules that elastically scatter with the faster flowing D–T ions producing a fast flowing molecule that strikes the surface. This does not happen at higher plasma temperatures because the molecules are rapidly dissociated by electrons and so do not remain intact. It should be noted that the effect of the high molecular flux on the ion parameters, if any, has not been self-consistently computed. In addition, improved molecular transport calculations, using improved dissociation and scattering cross sections, are required and are being planned.

3.4. Wall erosion

Fig. 4 shows the net erosion rate along the first wall for beryllium, carbon, and vanadium coatings. Tungsten erosion is zero and so is not shown. The distance parameter follows the curved boundary surface shown in Fig. 1, with distance measured from bottom-to-top of the machine with $x=0$ being the divertor/wall transition

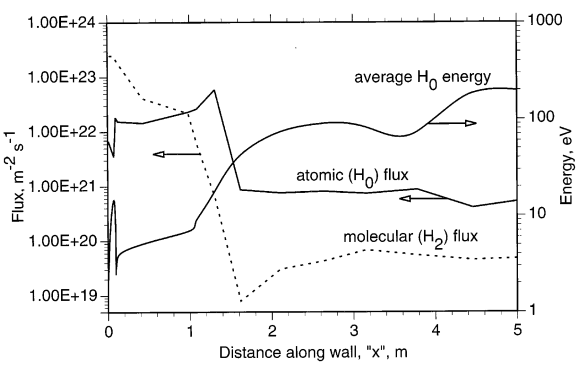

Fig. 3. Charge exchange atomic and molecular fluxes and average atomic energy to the first wall. For the ITER detached plasma regime. 'H' denotes D or T hydrogen isotope.

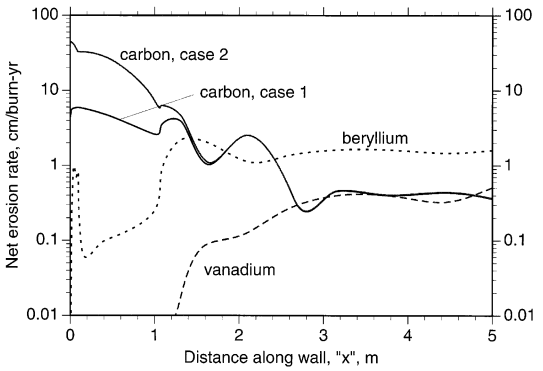

Fig. 4. Net erosion profile along the first wall, for the ITER detached plasma regime.

point, and $x = 5$ m being near the midplane. The baffle and limiter are therefore sequentially encountered with increasing x.

For beryllium and vanadium, most wall sputtering is due to charge exchange neutrals with only a small ion contribution. For carbon, chemical sputtering is important. Indeed, a key difference between beryllium and carbon, for detached conditions, is the lack of chemical sputtering for beryllium. For all physically sputtered material there is little redeposition on the wall. This is due to the low plasma density and temperature near the wall. There are simply too few higher energy electrons in the near-surface plasma to ionize many sputtered atoms. (The typical sputtered Be atom near-surface ionization mean free path exceeds 10 cm). Also, the plasma density is too low for significant near-surface elastic collisions between D–T ions/atoms and the physically sputtered atoms. For physically sputtered material, therefore, the gross and net erosion rates are approximately equal.

For chemically sputtered carbon at the 1–2 eV detached plasma temperatures, proton impact processes dominate the hydrocarbon transport with electron impact ionization again being negligible. It is found from the WBC calculations that about 50% of the chemically sputtered carbon from the wall surfaces is immediately (i.e. due to near-surface transport) redeposited. This is much lower than the $\sim 90\%$ redeposition fraction found at the divertor [1]. The key difference is the lower plasma density at the wall compared to the divertor, with second order differences due to the near-parallel wall field line structure. The present results also contrast with the near 100% redeposition found for non-detached regimes [18].

The two carbon cases shown in Fig. 4 differ by the assumed value of the non-thermal D–T molecular chemical sputtering coefficient. Although thermal hydrogen molecules do not react with graphite, impinging fast molecules may chemically sputter due to the resulting surface-dissociated, slightly energetic (several eV), hydrogen atoms. The non-thermal molecular yields are taken as $Y_{\mathrm{mol}} = 0.001$ for 'Case 1' and $Y_{\mathrm{mol}} = 0.01$ for 'Case 2'. In both cases the ion and atom chemical sputtering coefficient is 0.01. These values are all highly uncertain. Some discussion of the chemical sputtering yield issue is given in Ref. [1]. As shown, there is about a factor of 10 difference in the peak carbon erosion rate between the two cases.

For tungsten there is essentially no sputtering of wall components for this detached regime—impinging D–T particle energies are lower than the sputtering threshold energies (except for an extremely small high energy tail of the distribution). This is also true for impinging helium ions. Tungsten sputtering by any plasma radiating impurities, such as neon, were not considered here but should be low for this plasma regime. For the present purposes the net erosion rate for iron, representing a bare stainless steel wall, can be taken as equal to the vanadium rate.

3.5. Tritium codeposition

Table 2 shows the rate of tritium codeposition on ITER plasma facing surfaces due to first wall sputtering. The rate is shown as a function of a parametrized, spatially-constant surface temperature. The temperatures used span the range of most areas of the divertor. This is a rough calculation for scoping purposes only. Assumptions used for the computation are: (1) all non-wall redeposited material goes to the various divertor surfaces (target plate, pumping ducts, etc.). (This is plausible due to the structure of the plasma solution which suggests ionization of wall-sput-

tered material at higher temperature regions of the scrapeoff layer and subsequent transport along field lines to the divertor); (2) such redeposited material grows on the surfaces, i.e. no further erosion is assumed; and (3) the D–T flux to the growing surfaces is high enough and energetic enough to cause saturation of the surface with hydrogen isotopes up to the temperature-dependent saturation value.

The tritium calculation for Be uses two models for temperature-dependent H-isotope to Be trapping ratios. For 'Case 1', we use data directly, or linearly scaled, from the Tritium Plasma Experiment (TPE) facility results [1]. These H/Be trapping ratios are 0.35 for 100°C, 0.15 for 200°C, 0.03 for 300°C, and (by linear projection) 0.00 for 400°C. For 'Case 2' we use data from Mayer et al. [27] with a temperature-dependent correction factor to account for a reported C/Be content of $\sim 15\%$. The resulting H/Be trapping ratios for 'non-carbon-containing' beryllium are 0.28 for 150°C, 0.27 for 200°C, 0.14 for 300°C, and 0.10 for 400°C.

Hydrogen trapping fractions for carbon are given by the model of Ref. [28]. For vanadium the present assumption, pending a better estimate currently being assessed, is that the H/V values are the same as the Case 1 H/Be values.

Table 2
Scoping calculation—tritium codeposition rate in redeposited divertor-region surface layers, due to erosion of the ITER first wall

Wall material	Codeposition rate, g-T/1000 s pulse @surface temperature (°C)			
	150	200	300	400
Carbon[a]	23	21	15	9
Beryllium, Case 1[b]	14	9	2	0
Beryllium, Case 2[c]	16	15	8	6
Vanadium[d]	2	1	0.3	0
Tungsten	0	0	0	0

For the detached plasma regime of Ref. [16]. For lower-half first wall erosion only. Includes inner wall erosion using simple geometric scaling of outer wall results. Rate computed as a function of fixed surface temperature of redeposited surface.
[a] Case 1.
[b] H/Be codeposition ratio from TPE data [1].
[c] H/Be codeposition ratio from Mayer et al. [27].
[d] For hydrogen codeposition ratio same as beryllium Case 1.

Table 2 shows high tritium codeposition rates for carbon for the conditions studied. They are high for beryllium for surface temperatures of 200°C or lower. At higher surface temperatures the predicted codeposition rate depends critically on the data source used, with the TPE data showing little or no codeposition and the Mayer et al. [27] data showing reduced but still significant retention. For vanadium, based on the present assumption, the tritium retention is about one tenth that for beryllium—this follows from the factor-of-ten less total erosion.

4. Discussion

A major uncertainty in the hydrogen/beryllium trapping data is the effect of oxygen on beryllium codeposition properties. There is recent TPE data (R. Causey, Sandia National Laboratories, personal communication) indicating that redeposited beryllium in the absence of oxygen, traps considerably less hydrogen, thereby implying a rate controlling role for oxygen, via the formation of BeO. At present the effect of oxygen on the redeposited beryllium surface, and likewise, the amount of and effect of oxygen in ITER is uncertain and must be resolved with further study. A further issue is the effect of incident particle energy on trapping and in particular the role of codeposition vs. coimplantation, the latter involving higher energy particles. Finally, the effects of mixed materials, such as beryllium-carbon layers, on sputtering and codeposition properties, may be significant.

5. Conclusions

This paper has reviewed several past studies of beryllium sputtering erosion in fusion reactors, has presented new calculations of low energy oblique incidence beryllium sputtering yields, and has discusssed erosion results for a previously unanalyzed edge regime—that of a detached plasma.

For the ITER detached plasma edge regime, it was previously found [1] that erosion of a beryl-

lium coated divertor target may be small or even zero. However, as shown here, erosion of the first wall will be non-zero due primarily to an energetic charge exchange flux, together with low redeposition rates. Beryllium erosion is either roughly comparable to carbon or about 10 times lower in peak rate, depending on the assumed non-thermal molecular sputtering coefficient of carbon. Vanadium (or iron) peak erosion is about 10 times lower than beryllium. Tungsten erosion is negligible. Along with the erosion of the low-Z materials, there is a serious concern about tritium trapping in redeposited material. However, a far more detailed analysis of plasma-transported sputtered material, as well as significantly more H/Be trapping data regarding, in particular, the effect of oxygen on trapping, mixed material effects, and high temperature behavior, is needed to see if this is a real concern for beryllium.

From the standpoint of erosion and tritium trapping, beryllium would appear to be a better choice than carbon as a wall coating material for a detached plasma regime. If the $\sim$1-m long near-divertor-target region were excluded (such region being nominally tungsten coated in the present ITER design) the choice would be less clear. In general, however, beryllium erosion performance is roughly similar to carbon and much inferior to high-Z materials, for most of the regimes studied. Ultimately, use of beryllium (or carbon) in commercial reactors appears to be highly questionable, unless very different plasma regimes, such as with very high edge temperatures, can be obtained.

References

[1] J.N. Brooks, R. Causey, G. Federici, D.N. Ruzic, J. Nucl. Mater. 241–243 (1997) 294.
[2] J.N. Brooks, Nucl. Technol./Fusion 4 (1983) 33.
[3] J.N. Brooks, in: R.K. Janev, H.W. Darwin (Eds.), Atomic and Plasma-Material Interaction Processes in Controlled Thermonuclear Fusion, Elsevier, Amsterdam, 1993, p. 403.
[4] J.N. Brooks, Fusion Technol. 18 (1990) 239.
[5] J.N. Brooks, Phys. Fluids 8 (1990) 1858.
[6] T.Q. Hua, J.N. Brooks, Phys. Plasmas 1 (1994) 3607.
[7] D.N. Ruzic, Nucl. Instrum. Methods B47 (1990) 118.
[8] R.B. Turkot Jr., Ph.D. Thesis, Department of Nuclear Engineering, University of Illinois, 1996.
[9] R.T. McGrath, J.N. Brooks, J. Nucl. Mater. 162–164 (1989) 350.
[10] C.P.C. Wong, et al., J. Nucl. Mater. 196–198 (1992) 871.
[11] T.Q. Hua, J.N. Brooks, J. Nucl. Mater. 220–222 (1995) 342.
[12] M.J. Khandagle, Y. Hirooka, R.W. Conn, J.N. Brooks, A. Hassanein, R.B. Turkot Jr., J. Nucl. Mater. 207 (1993) 116.
[13] D. Naujoks, J. Roth, K. Krieger, G. Lieder, M. Laux, J. Nucl. Mater. 210 (1994) 43.
[14] J.N. Brooks, Proc. 16th IEEE/NPSS, IEEE no. 95CH35852, 1995, p. 1279.
[15] J.N. Brooks, D.N. Ruzic, D.B. Hayden, R.B. Turkot Jr., J. Nucl. Mater. 220–222 (1995) 269.
[16] K.J. Dietz, et al., Fusion Eng. Design 27 (1995) 96.
[17] A. Kukushkin, et al., J. Nucl. Mater. 241–243 (1997) 268.
[18] J.N. Brooks, ANL/FPP/TM-259, 1992.
[19] A.B. Ehrhardt, W.D. Langer, PPPL-2477, 1987.
[20] W. Wang, W. Eckstein, R. Schwörer, H. Plank, J. Roth, J. Nucl. Mater. 220–222 (1995) 1033.
[21] D.N. Ruzic, Phys. Fluids B5 (1993) 3140.
[22] R. Chodura, Physics of plasma—wall interactions in controlled fusion, in: D.E. Post, R. Behrish (Eds.), Controlled Fusion, Plenum, New York, 1986, p. 99.
[23] J.P. Biersack, W. Eckstein, Appl. Phys. 34 (1984) 73.
[24] P.C. Smith, Ph.D. Thesis, Department of Nuclear Engineering, University of Illinois, 1997.
[25] D.N. Ruzic, P.C. Smith, R.B. Turkot Jr., J. Nucl. Mater. 241–243 (1997) 1170.
[26] D.N. Ruzic, Plasma Sci. 24 (1996) 81.
[27] M. Mayer, R. Behrish, H. Plank, J. Roth, G. Dollinger, C.M. Frey, J. Nucl. Mater. 230 (1996) 67.
[28] J.N. Brooks, H.F. Dylla, A.E. Pontau, K.L. Wilson, Fusion Technol. 19 (1991) 1095.

.